Myoconductive and osteoinductive free-standing polysaccharide membranes

Sofia G. Caridade [a,b,c,1], Claire Monge [c,d,1], Jorge Almodóvar [c,d,2], Raphael Guillot [c,d], Jonathan Lavaud [e], Véronique Josserand [e], Jean-Luc Coll [e], João F. Mano [a,b,*], Catherine Picart [c,d,*]

[a] 3B's Research Group – Biomaterials, Biodegradables and Biomimetics, University of Minho, Headquarters of the European Institute of Excellence on Tissue Engineering and Regenerative Medicine, AvePark, Zona Industrial da Gandra, S. Cláudio do Barco, 4806-909 Caldas das Taipas, Guimarães, Portugal
[b] ICVS/3B's – PT Government Associate Laboratory, Braga/Guimarães, Portugal
[c] CNRS, UMR 5628, LMGP, 3 parvis Louis Néel, F-38016 Grenoble, France
[d] Université de Grenoble Alpes, Grenoble Institute of Technology, 3 parvis Louis Néel, F-38016 Grenoble, France
[e] Institute Albert Bonniot, INSERM U823, ERL CNRS3148, Grenoble, France

ABSTRACT

Free-standing (FS) membranes have increasing applications in the biomedical field as drug delivery systems for wound healing and tissue engineering. Here, we studied the potential of free-standing membranes made by the layer-by-layer assembly of chitosan and alginate to be used as a simple biomimetic system of the periosteum. The design of a periosteum-like membrane implies the elaboration of a thick membrane suitable for both muscle and bone formation. Our aim was to produce well-defined ~50 μm thick polysaccharide membranes that could be easily manipulated, were mechanically resistant, and would enable both myogenesis and osteogenesis in vitro and in vivo. The membranes were chemically crosslinked to improve their mechanical properties. Crosslinking chemistry was followed via Fourier transform infrared spectroscopy and the mechanical properties of the membranes were assessed using dynamic mechanical analysis. The loading and release of the potent osteoinductive growth factor bone morphogenetic protein 2 (BMP-2) inside and outside of the FS membrane was followed by fluorescence spectroscopy in a physiological buffer over 1 month. The myogenic and osteogenic potentials of the membranes in vitro were assessed using BMP-2-responsive skeletal myoblasts. Finally, their osteoinductive properties in vivo were studied in a preliminary experiment using a mouse ectopic model. Our results showed that the more crosslinked FS membranes enabled a more efficient myoblast differentiation in myotubes. In addition, we showed that a tunable amount of BMP-2 can be loaded into and subsequently released from the membranes, depending on the crosslinking degree and the initial BMP-2 concentration in solution. Only the more crosslinked membranes were found to be osteoinductive in vivo. These polysaccharide-based membranes have strong potential as a periosteum-mimetic scaffold for bone tissue regeneration.

© 2015 Acta Materialia Inc. Published by Elsevier Ltd. All rights reserved.

1. Introduction

Bone structure is characterized as a complex 3-D tissue composed of cells and mineralized extracellular matrix. Ongoing research in the field of biomaterials aims to better mimic the properties of natural tissues [1] and to guide cell fate locally for the regeneration of damaged tissues [2]. There are several membrane-like native tissues, which have important physiological roles. For instance, the periosteum—or pericranium for the skull—is a thick membrane covering the outer surface of all bones except at sites of articulation [3]. It consists of an outer fibrillar layer and

* Corresponding authors at: 3B's Research Group – Biomaterials, Biodegradables and Biomimetics, University of Minho, Headquarters of the European Institute of Excellence on Tissue Engineering and Regenerative Medicine, AvePark, Zona Industrial da Gandra, S. Cláudio do Barco, 4806-909 Caldas das Taipas, Guimarães, Portugal. Tel.: +35 12 53 51 09 00; fax: +35 12 53 51 09 09 (J.F. Mano). CNRS, UMR 5628, LMGP, 3 parvis Louis Néel, F-38016 Grenoble, France. Tel.: +33 4 56 52 93 11; fax: +33 4 56 52 93 01 (C. Picart).

E-mail addresses: jmano@dep.uminho.pt (J.F. Mano), catherine.picart@grenoble-inp.fr (C. Picart).

[1] Co-first authors; these authors contributed equally.
[2] Current address: University of Puerto-Mayagüez, Department of Chemical Engineering, PO Box 9000, PR 00681-9000, Puerto Rico.

an inner cellular layer, the thickness of which varies according to age and species (eg 40 μm for mouse tibiae [4], 100 μm for human tibiae [5] and 200 μm for pig mandible [6]). The periosteum constitutes a niche for many cells that participate in ossification during prenatal development and fracture healing [7–9]. As the periosteum is widely recognized to be of critical importance in bone formation and regeneration, the development of a periosteum-like membrane would be a promising strategy for bone tissue engineering [10,11]. There are only a few models of periosteum for engraftment in bone defects, including natural scaffolds such as porcine small intestinal submucosa [12], decellularized periosteum [13] and vascularized biomimetic cell-sheet-engineered periosteum [14].

In the past few years, a periosteum-like environment has been developed using electrospun hydroxyapatite-containing chitosan (CHI) nanofibers [15]. Polyethylene glycol hydrogels have also been used to emulate the periosteum in a murine femoral defect model [16]. Recently, free-standing (FS) microgrooved poly(lactic-co-glycolic acid) nanosheets have been developed for the purpose of generating a biomimetic periosteum [11]. Since the muscle–periosteum connection is important for periosteal healing [17], the design of a periosteum-like membrane implies the elaboration of a thick membrane suitable for both muscle and bone formation.

The layer-by-layer (LbL) technique appears to be a powerful tool for the engineering of FS membranes. LbL coatings offer a large range of potentialities for biomedical applications [18–21]. Their thickness and internal structure can be easily tuned, depending on the molecules used as building blocks [22], the number of layers deposited and the assembly conditions (pH, ionic strength, concentration of the polyelectrolytes). Several physico-chemical and mechanical parameters can be directly controlled, including ion permeation [23], crosslinking of the films (which changes their Young's modulus [24] but also their biodegradability properties [25]) and loading of bioactive molecules [26].

To date, few studies have reported the production of polysaccharide-based FS membranes constructed via the LbL technique [27–29]. Interestingly, these FS membranes can be simply obtained using a bottom-up approach by depositing oppositely charged polysaccharides and then removing the underlying substrate [27]. When the film is deposited on a low surface energy substrate, it can be removed in mild conditions, leading an FS membrane without the need for a post-processing step [28,29].

Polysaccharides can interact, via non-covalent interactions, with several growth factors [30,31] that can stimulate cellular proliferation, migration and differentiation. Furthermore, trapping growth factors in a biomimetic matrix can provide a sustained release at a lower dose [32]. Indeed, hydrogels based on CHI and alginate (ALG) have already been used as a delivery carrier for bone morphogenetic protein 2 (BMP-2) [30].

In our previous study [29], we engineered thick FS membranes (4–35 μm) made of CHI and ALG by tuning the following deposition conditions: pH, polyelectrolyte concentration and number of deposited layer pairs. These FS membranes were stable in a physiological buffer and enabled the partial permeation of model drugs, indicating that they may act as a reservoir for bioactive proteins. Furthermore, we showed that these membranes enabled the growth of skeletal myoblasts (C2C12), though with differences depending on the chemistry of the ending layer.

In this work, we further explored the potentiality of the FS CHI/ALG membranes as a simple model of a natural periosteum membrane. We generated FS CHI/AGL membranes with tunable mechanical properties, as confirmed by dynamic mechanical analysis, modulated by chemical crosslinking. BMP-2 was then incorporated into these membranes, and its release was followed for 1 month. Lastly, the bioactivity of these membranes towards both myogenesis and osteogenesis was assessed in vitro using skeletal myoblasts and their bioactivity in vivo was assessed using an ectopic mouse model.

2. Materials and methods

2.1. Materials

CHI (medium molecular weight) was purchased from Sigma–Aldrich (Germany) and was purified prior to use by a reprecipitation method [33]. Briefly, the CHI was purified by dissolving it in acetic acid and then precipitating it with NaOH (final pH ∼8). The suspension was subsequently sieved, and the precipitate was thoroughly washed with distilled water and rinsed twice with ethanol for about 4 h. The product was frozen at −80 °C and lyophilized. Finally, the obtained product was milled and the CHI powder was dried at 60 °C overnight. The degree of N-deacetylation was found to be 78% by first-derivative ultraviolet spectrophotometry, using both glucosamine and N-acetylglucosamine standards for calibration [34]. The molecular weight (M_v) was determined by viscometry in 0.5 M CH_3COOH/0.2 M $NaCH_3COO$, and was found to be 770 kDa according to the Mark–Houwing theory ($k = 3.5 \times 10^{-4}$; $a = 0.76$) [35]. The CHI was fluorescently labeled using Alexa 568 (Invitrogen) following the manufacturer's protocol, except that the reaction was carried out for 2 h at pH 6 [29]. A Sephadex G-25 size exclusion column (PD-10, Amersham Bioscience, Sweden) was used to purify the product and remove any unbound dye.

Sodium ALG, derived from brown algae (low viscosity: 136 mPa.s), was obtained from Sigma and used as received. Human recombinant BMP-2 was provided by Medtronics. BMP-2 labeled with carboxyfluorescein ($BMP-2^{CF}$) was used to visualize BMP-2 in FS membranes as well as to quantify its incorporation by fluorescence spectrometry [26]. All reagents and solvents were used without further purification. For staining of the cells, rhodamine phalloidin (P2141) and the anti-troponin T antibody (T6277) were purchased from Sigma. The 5-ethynyl-2′-deoxyuridine (EdU) proliferation assay (C10340) was purchased from Life technologies.

2.2. Preparation of thick (CHI/ALG) free-standing films

The different steps of the FS membrane preparation are summarized in Scheme 1. Briefly, the multilayer films were built on polypropylene substrates using freshly prepared polyelectrolyte solutions (step 1). Prior to film deposition, the substrates were cleaned with ethanol and rinsed thoroughly with water before being dried with a stream of nitrogen. The substrates were first dipped in the CHI solution for 5 min, then rinsed twice in water (both at pH 5) for 2 min. Subsequently, they were immersed in ALG solution (pH 3) for 5 min, followed by rinsing twice in water (with the same pH as the ALG solution) for 2 min [29]. This procedure was repeated using a dipping robot (DR3, Kirstein and Viegler GmbH) until the deposition of 200 layer pairs had been achieved. These FS membranes are hereinafter referred to as $(CHI/ALG)_{200}$. The membranes were subsequently allowed to dry in air and detached from the substrates. For membrane crosslinking (step 2), 1-ethyl-3-(3-dimethylaminopropyl)carbodiimide hydrochloride (EDC) and N-hydroxysulfosuccinimide (s-NHS) were dissolved in Milli-Q water, pH 5.5, at final concentrations of 10, 30, 50 mg ml^{-1} (for EDC) and 11 mg ml^{-1} (for s-NHS), respectively. The FS membranes were put in contact with the freshly prepared EDC/s-NHS solution overnight at 4 °C. They were then thoroughly washed with HEPES (20 mM) at pH 7.4 and dried at room temperature. In the following, the FS membranes crosslinked with EDC at 10, 30 and 50 mg ml^{-1} are denoted EDC10, EDC30 and EDC50, respectively.

3
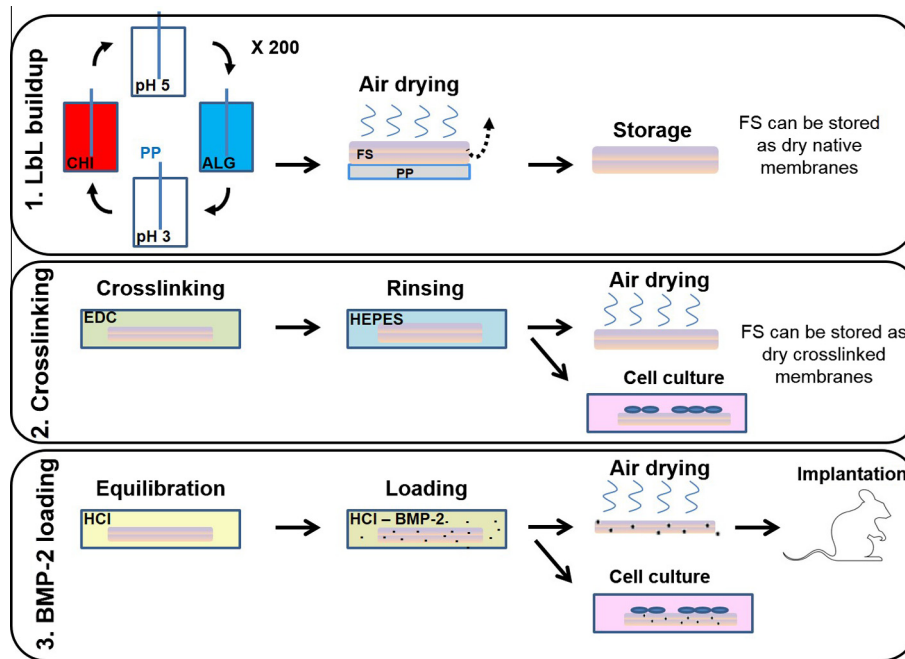
Scheme 1. Different steps of the preparation of the (CHI/ALG)$_{200}$ FS membranes. 1. The film is built on a polypropylene (PP) substrate before being air dried, detached and stored. 2. The FS membrane is crosslinked using EDC and rinsed; it is then used for the myoblast culture. 3. The FS membrane is subsequently loaded with BMP-2; its osteoinductive properties are assessed in vitro and in vivo in mice. After steps 2 and 3 of the procedure, the FS membrane can be stored in a dry state.

2.3. Fourier transform infrared spectroscopy (FTIR)

The chemical structure of the dry FS membranes was studied by FTIR in transmission mode using a Vertex 70 spectrophotometer (BrukerOptic Gmbh, Ettlingen, Germany) equipped with a mid-infrared detector [36]. All spectra were recorded between 400 and 4000 cm^{-1} with a 2 cm^{-1} resolution, using Blackman–Harris three-term apodization and the standard Bruker OPUS/IR software v6.5 (Bruker Optic Gmbh). After detachment of the FS membrane, the spectra of the uncrosslinked and crosslinked (CHI/ALG)$_{200}$ FS films were acquired and the spectrum of air was taken as a reference. The experiments were performed in duplicate, with at least four different samples per condition in each independent experiment.

2.4. Scanning electron microscopy (SEM)

The morphological analysis of the uncrosslinked and cross-linked (CHI/ALG)$_{200}$ FS membranes was performed using SEM (Quanta FEG 250 FEI), with both sides of the membranes being observed in a high vacuum with a Everhart–Thornley detector for secondary electrons at an acceleration of 3 kV. For cross-section observations, the FS membranes were dipped in liquid nitrogen until freeze fracture and the morphology was observed.

2.5. Dynamic mechanical analysis (DMA)

All viscoelastic measurements were performed using a Tritec2000B dynamic mechanical analyser (Triton Technology, UK) in the tensile mode. The measurements were carried out at 37 °C. The membrane samples were cut to ~4 mm width (measured accurately for each sample). Uncrosslinked and crosslinked (CHI/ALG)$_{200}$ FS membranes were always analyzed immersed in phosphate-buffered saline (PBS) placed in a Teflon® reservoir. The geometry of the samples was then measured and the FS membranes were clamped in the DMA apparatus at a spacing of 10 mm and immersed in the liquid bath. After equilibration at 37 °C, the

DMA spectra were obtained from a frequency scan between 0.1 and 10 Hz. A static preload of 1 N was applied during the tests to keep the sample tight. Three specimens were tested for each condition.

2.6. BMP-2 loading and release

For the adsorption of BMP-2 on the FS membranes (Scheme 1, step 3), a previously established protocol was followed [26,37]. Briefly, the FS membranes were cut into samples (~1 cm^2) and deposited into 24-well plates, where they were immersed in a 1 mM HCl solution (pH 3) for about 1 h. After removal of the HCl solution from the wells, the FS membranes were incubated with the BMP-2 solution (overnight and at 4 °C). For the in vitro studies, the loading was performed with a BMP-2 solution containing 2% BMP-2^{CF}. The FS membranes were incubated at several concentrations of BMP-2 (20, 60 and 100 µg ml^{-1}) and their release profiles were investigated. For EDC30, the loading was only performed at 20 µg ml^{-1}. Quantification of BMP-2 loading in and release from the FS after several washes with a HEPES buffer (20 mM, pH 7.4) was determined using a fluorescence spectrometer (Tecan Infinite 1000, Austria), as previously described [26]. Briefly, after the BMP-2 loading solution had been removed from the wells, the HEPES solution was added and the fluorescence of the well (including FS membrane + HEPES solution) was measured (excitation 492 nm/emission 517 nm). At predetermined intervals, the HEPES solution in the wells was replaced by fresh HEPES solution and the fluorescence was measured. The amount incorporated was calculated based on a calibration curve obtained with known amounts of BMP-2 in solution (data not shown). The experiments were performed in duplicate, with three different samples for each condition in each independent experiment.

2.7. Cell culture

Murine C2C12 skeletal myoblasts (<20 passages, obtained from the American Type Culture Collection) were cultured in tissue

culture flasks in a 1:1 Dulbecco's modified Eagle's medium/Ham's F12 medium (DMEM/F12; Gibco, Invitrogen, Cergy-Pontoise, France) supplemented with 10% fetal bovine serum (PAA Laboratories, Les Mureaux, France) containing 10 U ml^{-1} penicillin G and 10 µg ml^{-1} streptomycin (Gibco, Invitrogen) in a 37 °C/5% CO$_2$ incubator. This medium is hereinafter denoted growth medium (GM). Cells were subcultured prior to reaching 60–70% confluence (approximately every 2 days).

2.8. C2C12 cell adhesion, proliferation and differentiation

Cell adhesion was performed on $10 \times 10 \text{ mm}^2$ (CHI/ALG)$_{200}$ membranes. At confluence, cells were trypsinized and seeded onto the membranes at a density of 3×10^4 cells cm^{-1} in 500 µl of medium. For this purpose, the FS membranes were kept at the bottom of the wells using a silicone ring. The cell suspension was added on top of each immobilized membrane. In these culture conditions, the medium was able to diffuse through the membrane. To commit C2C12 cells toward myogenic differentiation, the cell medium was switched from GM to a differentiation medium (DM; (1:1 DMEM/F12) supplemented with 2% horse serum, containing 10 U ml^{-1} penicillin G and 10 µg ml^{-1} streptomycin.

For fluorescent staining of the cells and myotubes, C2C12 myoblasts were fixed in a solution of 3.7% of formaldehyde in Tris–NaCl buffer (0.15 M NaCl, 50 mM Tris–HCl, pH 7.4; TBS) for 20 min and permeabilized for 4 min in TBS containing 0.2% Triton X-100. Samples were blocked in TBS containing 0.1% BSA for 1 h, and then incubated with mouse anti-troponin T (1:100) antibody in TBS containing 0.2% gelatin for 30 min. AlexaFluor488-conjugated secondary antibody was then incubated for 30 min. The actin cytoskeleton was stained by incubation in phalloidin–rhodamine (1:800) for 30 min and nuclei were stained with 0.5 µg ml^{-1} 4′,6-diamidino-2-phenylindole (DAPI). The fusion index of the myotubes was calculated based on troponin T, as previously described [38]. Briefly, the fusion index represents the proportion of fusion events that occurs in a given condition. The higher the fusion index, the more myoconductive the substrate. It was determined by dividing the total number of nuclei in the myotubes (minimum of two nuclei) by the total number of nuclei counted [38]. The results represent at least three independent experiments, with three FS membranes per condition. More than 100 nuclei were analyzed for each condition.

The proliferation assay is based on the incorporation of the modified RNA nucleoside uridine (5-ethynyl-2′-deoxyuridine, EdU). During EdU assay, the dividing cells were stained and thus quantified to rate the proliferation of cells onto the membranes. The cells were then exposed to 10 µM EdU in culture medium for 30 min, fixed and permeabilized, and stained according to the manufacturer instructions. Experiments were performed in triplicate, with three different samples for each condition in each experiment.

2.9. Alkaline phosphatase (ALP) assay and mineralization assay

ALP is an early marker of osteogenic differentiation. The ALP assay determines the quantitative amount of ALP expressed by the cells, which reflects their commitment to the osteogenic pathway. BMP-2 bioactivity was assayed on C2C12 cells by quantifying their ALP expression. C2C12 cells were seeded at 90,000 cells ml^{-1} of GM onto BMP-2-loaded membranes (20 µg ml^{-1}) deposited in 24-well plates. After 3 days of culture, the culture medium was removed and the cells were washed with PBS and lysed by sonication over 5 s in 500 µl of 0.1% Triton-X100 in PBS. Next, 180 µl of a pH 10 buffer containing 0.1 M 2-amino-2-methyl-l-propanol (Sigma, France), 1 mM MgCl$_2$, and 9 mM p-nitrophenyl phosphate (Euromedex, France) was added to 20 µl of this lysate. The enzymatic reaction was monitored in a 96-well plate by measuring the absorbance at 405 nm using a Tecan Infinite 1000 microplate reader (Tecan, Austria) over 10 min. The total protein content of each sample was determined using a bicinchoninic acid based protein assay kit (Interchim, France). The ALP activity was expressed as millimoles of p-nitrophenol produced per minute per milligram of protein. The experiments were performed for cells grown on BMP-2-loaded membranes (bBMP-2) crosslinked to different extents (EDC10, 30 and 50). A positive control was also included by adding BMP-2 in solution (sBMP-2) for cells loaded on the unloaded FS membranes. The experiments were performed in triplicate, with three different samples for each condition in each independent experiment.

For mineralization, C2C12 cells were cultured on the FS membranes (loaded or not with BMP-2) for 2 weeks in GM supplemented with 50 mM ascorbic acid and 8 mM β-glycerol phosphate. Alizarin red staining was used to detect mineralization. Cells were fixed in 3.7% formaldehyde in PBS for 40 min. After rinsing with milliQ water, 500 µl of Alizarin red (2% w/v in water, pH 4.2, adjusted with NaOH and HCl) was added to each sample and incubated at room temperature for 30 min then rinsed with Milli-Q water. Images were taken using an Olympus bx41 microscope. Alizarin staining was quantified by converting the uncalibrated linear RGB pictures into an uncalibrated linear 32-bit CMYK stack using the plug-in version of Stephan Saalfeld's BeanShell script in the Image J software v1.43 m (NIH). The magenta picture was then taken as being the closest to red and the integrated density was determined for each condition.

2.10. Imaging of cells and FS membranes

Cells and membranes were observed using a Zeiss LSM 700 confocal laser scanning microscope (CLSM, Carl Zeiss SAS, Le Pecq, France) in the HEPES-NaCl with a 10× or 20× air immersion objective. The membranes were deposited in between two 25 mm diameter glass coverslips in a drop of HEPES 20 mM maintained by an Attofluor chamber (Invitrogen). All image quantifications were performed using Image J software v1.43 m (NIH).

2.11. Preliminary in vivo ectopic assay in mice

Two female NMRI nude mice (5 weeks old) weighing 24 ± 0.5 g were purchased from Janvier (Le Genest St Isle, France). Facility rooms were maintained at constant temperature and humidity (25 °C, 30–50% relative humidity), with a 12 h light/dark cycle. All animal studies were conducted in accordance with European Union guidelines and approved by the regional ethics committee. Four FS membranes crosslinked at EDC10 and EDC50 and loaded at two different BMP-2 amounts (60 and 100 µg ml^{-1}) (as described in Section 2.6) were used for the preliminary tests. The dry membranes were implanted subcutaneously into the backs of anesthetized mice. Anesthesia was performed using 1.5 l m^{-1} 4% isoflurane in air (Axience, Pantin, France) during induction and then 1 l m^{-1} 2% isoflurane in air for maintenance. After implantation, suture stitches were performed. Subcutaneous membrane-mediated bone formation was monitored at days 0, 9, 21, 32,42 and 52 post-implantation with whole-body scanner using micro-computed tomography (µCT; Viva-CT 40, Scanco Medical, Brütisselen, Switzerland) with low-resolution settings (an isotropic voxel size of 80 µm, a voltage of 70 kV and a current of 114 mA). Quantification of bone formation was obtained using a low threshold of

376 Q6 150 mg hydroxyapatite (HA) per cm^3. The region of interest was
377 drawn around the observed new bone formations.

378 ### 2.12. Statistical analysis

379 Data are reported as mean ± standard error of the mean and
380 statistical comparisons were performed using SigmaPlot software.
381 EdU, ALP and Alizarin red data were compared by t-test. For the
382 fusion index, as the numbers of cells for each condition were not
383 equal (there were much fewer cells in the EDC10 FS membranes),
384 a Mann–Whitney rank sum test was applied. All the conditions
385 for the released data (different EDC and different loading concen-
386 trations) were analyzed using a non-parametric Kruskal–Wallis
387 test. Statistically different values are reported in the figures
388 ($p < 0.05$ was considered significant).

389 ## 3. Results

390 ### 3.1. FS polysaccharide membranes: morphology and crosslinking

391 In this work, ∼50 µm thick FS membranes made of $(CHI/ALG)_{200}$
392 were produced by the LbL assembly of CHI and ALG on a polypro-
393 pylene substrate and subsequently detached by air drying. Such
394 membranes were easy to handle with tweezers in both dry and
395 hydrated conditions (Fig. 1A), and can be cut into any shape
396 desired. The $(CHI/ALG)_{200}$ FS membranes were crosslinked using
397 EDC in order to improve their stability in liquid conditions, as
398 LbL film stability and biodegradability can be significantly changed
399 by chemical crosslinking [28,39,40]. Interestingly, this chemistry is
400 of "zero length", meaning that there is no additional molecule
401 introduced into the film, the carbodiimide being simply converted
402 to a water-soluble urea derivative, which has very low cytotoxicity
403 [41,42] and can be washed away. SEM observations of the upper
404 side and cross-sections of the FS membranes crosslinked at
405 different degrees (Fig. 1B and B′) revealed an increased roughness
406 when the crosslinking degree was higher. Cross-sections of the
407 FS membranes (Fig. 1B′) also revealed the homogeneous structure
408 of the membranes.

409 Crosslinking of the FS membrane was characterized by FTIR and
410 DMA. Fig. 2A shows FTIR spectra of the $(CHI/ALG)_{200}$ membranes
411 crosslinked to different degrees. Two major regions can be

412 observed: a band at 1412 cm^{-1}, corresponding to the COO^- sym-
413 metric stretch of ALG [43]; and a second band between 1500 and
414 1700 cm^{-1}, containing the COO^- asymmetric stretch of ALG at
415 1605 cm^{-1} [44] and the amide I band of CHI. As the EDC concentra-
416 tion increased, we noted a broadening of the amine I band, a
417 decrease in the carboxylic peak at 1605 cm^{-1} and an increase in
418 the C = O ester band at 1736 cm^{-1} (Fig. 2A). Differences between
419 the spectra obtained after crosslinking to the spectrum of a native
420 membrane enabled us to highlight the structural changes upon
421 crosslinking, i.e. the increase in the amide I band and the decrease
422 in the COO^- peak (Fig. 2A′).

423 DMA experiments were performed to assess the mechanical/
424 viscoelastic behavior of the FS membranes in a physiological envi-
425 ronment (Fig. 2B and B′). The storage (elastic) modulus E' and the
426 loss factor (tanδ) were determined. E' was always lower than
427 3 MPa for the uncrosslinked membranes and the crosslinked mem-
428 branes at EDC10. In contrast, it was always higher than 15 MPa for
429 all the other crosslinking conditions. E' increased with increasing
430 EDC concentration except for the FS membranes at EDC70, which
431 were found to be brittle. We also noted a slight increase in E' with
432 increasing frequency, which has previously been found in pure CHI
433 membranes [45]. The tanδ value is the ratio of the amount of
434 energy dissipated by viscous mechanisms relative to energy stored
435 in the elastic component. It provides information about the damp-
436 ing properties of the membrane. The tanδ value was very similar
437 for all conditions, but it also exhibited a slight increase with
438 frequency. The native membrane and the EDC10 membranes had
439 slightly higher dissipative properties at these higher frequencies,
440 which can be related to their lower crosslinking degree [46].

441 Based on these results and on the fact that crosslinking is
442 known to improve resistance to factors such as pH changes and
443 enzymatic degradation [39], we selected FS membranes cross-
444 linked at EDC10, EDC30 and EDC50 for further cellular assays.

445 ### 3.2. Myogenic differentiation on crosslinked FS membranes

446 The C2C12 myoblasts were observed after 24 h in GM and after
447 5 days in DM (Fig. 3A). The percentage of proliferating cells and
448 their fusion index were quantified after 1 and 5 days, respectively
449 (Fig. 3B and C). We noted that few cells attached to the EDC10
450 membranes, whereas they adhered to and proliferated and fused
451 on the EDC30 and EDC50 membranes (Fig. 3A). The EdU prolifera-
452 tion assay confirmed that the cells were metabolically active and
453 exhibited significantly increased proliferation when the crosslink-
454 ing of the FS membrane was increased (Fig. 3B). After 5 days in DM
455 on EDC10 films, cells had begun to form large aggregates and there
456 was only a few short myotubes. However, cells differentiated into
457 long, thin myotubes on EDC30 and EDC50 crosslinked membranes
458 (Fig. 3C). The fusion index increased with the EDC concentration,
459 from 0.23 ± 0.11 for EDC10 to 0.41 ± 0.08 for EDC30 and 0.48 ±
460 0.03 for EDC50 FS membranes. All together, these results showed
461 that myogenic differentiation was influenced by the crosslinking
462 degree, the more crosslinked membranes being more
463 myoconductive.

464 ### 3.3. BMP-2 loading and release from the crosslinked FS membranes

465 In order to study the potentiality of the FS membranes for bone
466 repair, we selected BMP-2 as an osteoinductive growth factor
467 [47,48] to be loaded into the membranes. Here, we studied the
468 potentiality of crosslinked FS membranes to trap and subsequently
469 release BMP-2. CLSM images of the FS membranes after loading
470 with BMP-2 are shown in Fig. 4A, the FS membranes being labeled
471 in red with Alexa568. Two layers of BMP-2 were clearly visible at
472 the upper (ALG ending) and lower (CHI) sides of the membrane.
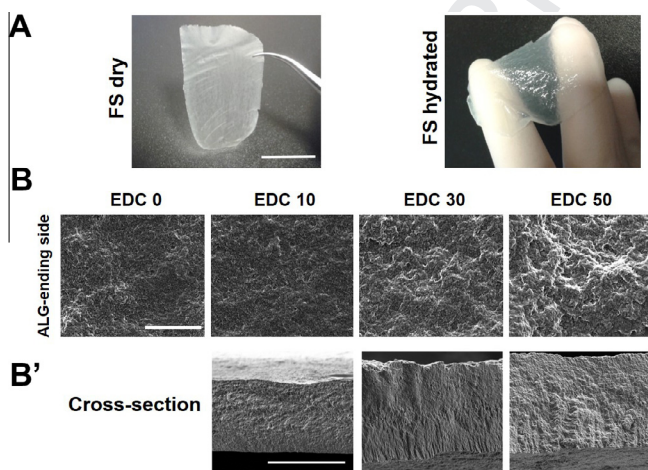473 Moreover, the BMP-2-loaded FS membranes were found to be

Fig. 1. Optical microscopy and SEM images of free-standing $(CHI/ALG)_{200}$ mem-
branes. (A) Images of a dry (left) or hydrated (right) $(CHI/ALG)_{200}$ FS membrane.
Scale bar = 1 cm. (B) SEM observations of the upper side of the native $(CHI/ALG)_{200}$
membrane and for the FS membranes crosslinked at increasing concentrations of
EDC from 10 to 50 mg ml^{-1}. Scale bar = 10 µm. (B′) Corresponding cross-sections of
the crosslinked FS membranes. Scale bar = 20 µm.

S.G. Caridade et al./Acta Biomaterialia xxx (2015) xxx–xxx
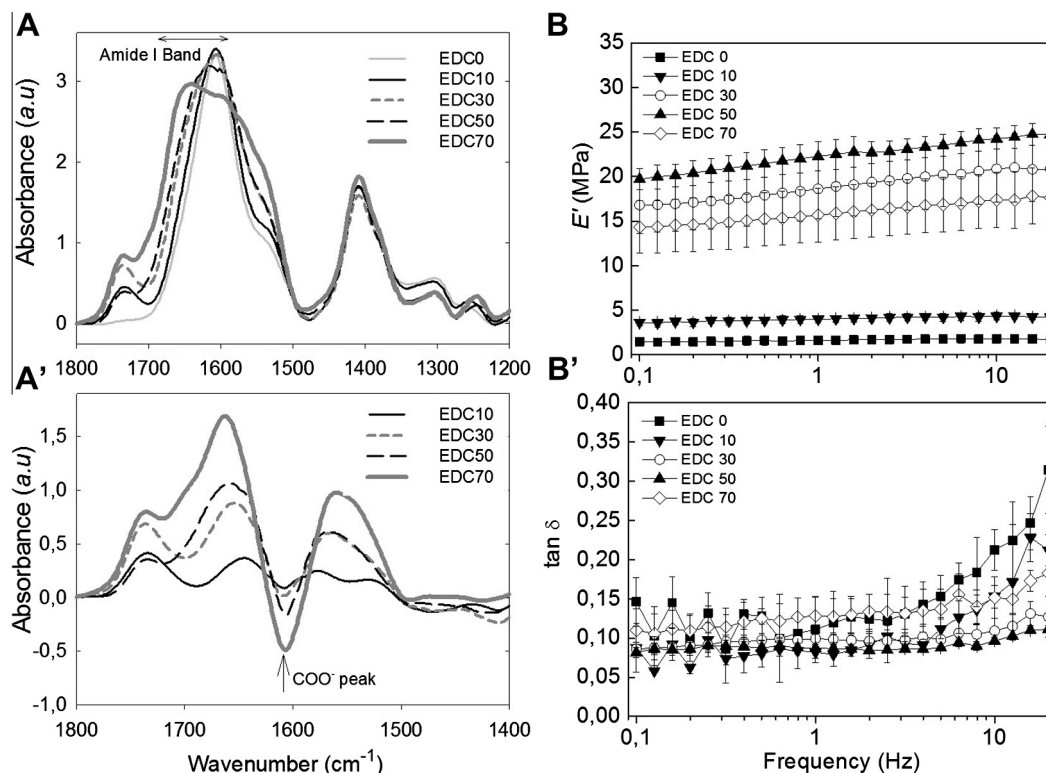
Fig. 2. Crosslinking and mechanical properties of the FS membranes. (A) FTIR spectra of native and crosslinked (CHI/ALG)$_{200}$ FS membranes obtained at increasing EDC concentrations and (A′) differences between the spectra of the crosslinked FS membranes to that of the native membrane. (B, B′) Results of the DMA experiments performed at 37 °C in PBS over 0.1–20 Hz. (B) Variation of the storage modulus (E′) and (B′) of the loss factor (tanδ).

stable and to retain their integrity when kept in HEPES at 4 °C for 8 months (Fig. 4A, right image).

The release kinetics of BMP-2 from the FS membranes was followed over 1 month for FS membranes loaded with BMP-2 at concentrations of 20, 60 and 100 µg ml^{-1} (Fig. 4B, B′ and B″ and Table 1). The incorporation of BMP-2 was measured initially (Γ_i) and after 1 month (Γ_f). For all the EDC concentrations, the amounts of BMP-2 incorporated, Γ_i, increased significantly with loading concentration of BMP-2. For instance, for the EDC10 membrane, the total amount of BMP-2 loaded increased from 2.7 to 10.8 µg when the initial BMP-2 concentration loaded increased from 20 to 100 µg ml^{-1}. Also, the initial loading of BMP-2 in the FS membranes was slightly higher for the EDC10 FS membranes than for the EDC50 FS membranes.

Regarding the release profiles, the trends were similar, with a "burst" release of ∼5–20% (Γ_b) observed in the first 4 h, followed by a continuous release until a plateau was reached. It should be noted that this burst was systematically higher for the low crosslinking membranes (EDC10) compared to the EDC50 ones. This was also the case for the absolute amount of BMP-2 released, which was of the order of 1–2 µg, and for the total percentage of BMP-2 released.

However, the final loaded amounts Γ_f of BMP-2 remaining in the FS after extensive washes were statistically similar for EDC10 and EDC50. Globally, Γ_f increased with the initial concentration of BMP-2 in solution. Maxima of 8.8 ± 2.3 and 7.4 ± 2.3 µg per membrane for EDC 10 and EDC 50, respectively, were reached for the highest loaded BMP-2 concentration of 100 µg ml^{-1}. The EDC30 FS membranes presented an intermediate trend and were not considered for further evaluation.

All together, these results showed that the amount of BMP-2 incorporated and the corresponding release profile can be tuned depending on the initial concentration of BMP-2 in solution and the degree of crosslinking of the FS membrane.

3.4. Osteoinductive potential of FS membranes in vitro and in vivo

The bioactivity of the BMP-2-loaded FS membranes in vitro was assessed using C2C12 myoblasts, these cells being an acknowledged model of osteoinduction in vitro [49]. We noted that cell adhesion slightly increased in the presence of bBMP-2 compared to sBMP-2 (data not shown). Cell proliferation, as quantified by the EdU assay (Fig. 5A), was only ∼4% for the EDC10 membranes, whereas it was significantly higher, at 17 ± 8 and 16 ± 6%, respectively, for the EDC30 and EDC50 FS membranes loaded with BMP-2. Regarding the osteogenic capacity of the FS membranes, we first verified, as a negative control, that all the crosslinked FS membrane did not induce ALP activity in the absence of BMP-2 (Fig. 5B and data not shown). The positive control consisted of sBMP-2 added to the cells grown on the crosslinked FS membranes. Cells were found to express a similar level of ALP on all the BMP-2-loaded FS membranes whatever the crosslinking degree, but the ALP level was lower than the positive control.

Longer term mineralization was also assessed after 1 and 2 weeks by visualizing Alizarin red staining (Fig. 5C and C′). As anticipated, only a very low basal staining of the membranes in the absence of BMP-2 was detected for all crosslinking conditions, as shown in Fig. 5C′ (and data not shown). In contrast, all BMP-2-loaded membranes induced a positive staining with Alizarin, indicating the presence of calcium deposits. The mineralization was visible at both time points. However, we noted significantly higher calcium deposition on EDC10 and EDC50 in comparison to EDC30 FS membranes. Overall, these results indicate that the BMP-2-loaded FS membranes are osteoinductive in vitro. As the two
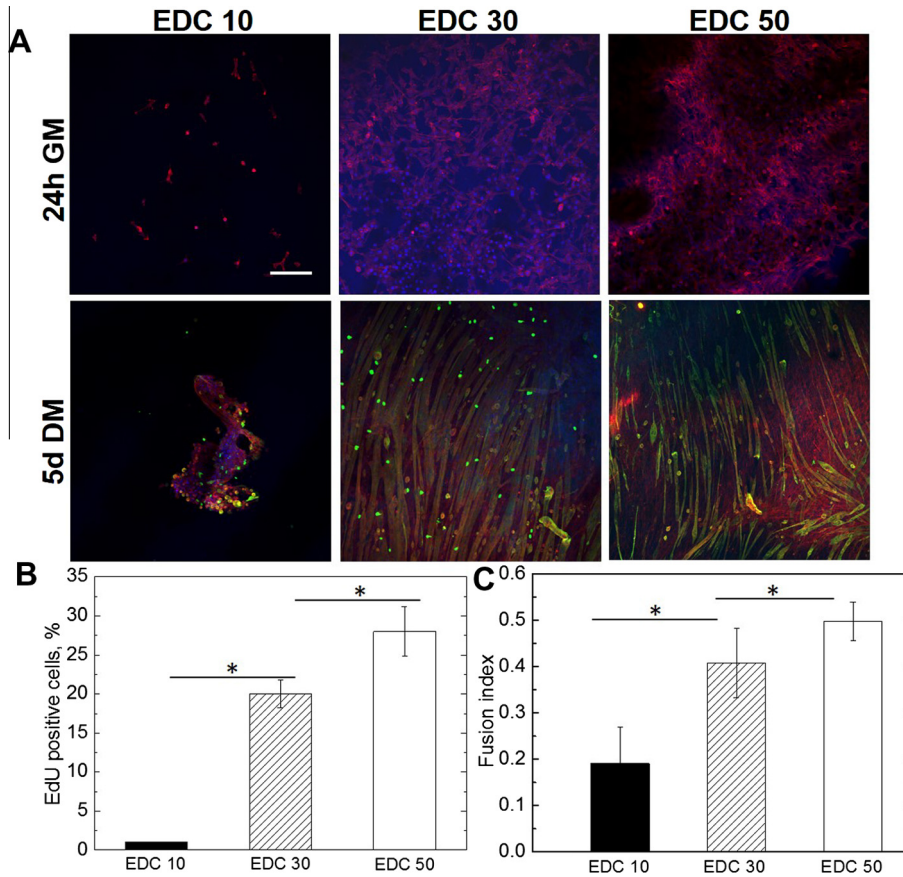
Fig. 3. C2C12 myoblast proliferation and differentiation on the FS polysaccharide membranes. Cells were cultured on the FS membranes crosslinked at EDC10, EDC30 and EDC50. (A) CLSM images of C2C12 myoblasts were taken after 24 h in GM and after 5 days in DM. The actin cytoskeleton was stained with rhodamine–phalloidin, the nuclei were stained with DAPI and the myotubes with troponin T. Scale bar = 200 μm. (B) Percentage of proliferating cells measured by the EdU assay after 24 h in GM and (C) quantification of the fusion index after 5 days in DM on EDC10, EDC30 and EDC50 FS membranes (mean + SEM of three independent experiments, $*p < 0.05$).

extreme conditions, ie EDC10 and EDC50, showed higher calcium deposition, we selected them for the in vivo preliminary study.

In order to further assess the osteoinductive potential of the BMP-2-loaded crosslinked FS membranes, a preliminary study was performed in vivo in a mouse ectopic model [50,51]. We selected four different FS membranes crosslinked at EDC10 and EDC50 and loaded at 60 and 100 μg ml^{-1}. In situ bone formation was followed by μCT for 8 weeks (Fig. 6A) and the bone volume was quantified (Fig. 6B). We noted that the EDC10 FS membrane did not lead to bone formation whatever the amount of BMP-2 loaded (Fig. 6 and data not shown). In contrast, a bone nodule was formed as soon as day 21 for the EDC50 FS membrane loaded with 100 μg ml^{-1} BMP-2, and this continued to grow up to day 52. These preliminary data suggest that only the EDC50 FS membrane loaded at the highest amount (100 μg ml^{-1}) exhibited osteoinductive properties in vivo.

4. Discussion

In this work, we developed a periosteum-like biomaterial by producing an ~50 μm thick FS membrane made of (CHI/ALG)$_{200}$ by LbL assembly. The periosteum being a bilayer structure, composed of a fibrous layer linking muscles and ligaments and a cellular layer of osteoblastic precursors [52], a biomimetic membrane would assume the characteristics of being both myoconductive and osteoinductive.

The development of skeletal muscle is a multistep process, which includes initial cell adhesion and proliferation, followed by withdrawal from the cell cycle and differentiation into multinucleated myotubes [53]. ALG has already been used as biomaterial for studying muscle cell growth [54–56]. Our previous work using C2C12 skeletal myoblasts cultured on ALG- or CHI-ending FS native membranes showed that cell adhesion was better on the ALG-ending membranes [29]. Here, we found that crosslinked FS membranes were myoconductive and that myoblast proliferation and differentiation increased as a function of the crosslinking degree. Our results are consistent with previous results showing that muscle cell adhesion, proliferation and differentiation depend on substrate stiffness [57–59]. It is important to note here that both the stiffness and the roughness may influence the cell fate, as we visualized by SEM that the surface of the FS membranes were rougher with a greater degree of crosslinking (Fig. 1B).

Delivering BMP-2 in a controlled manner is a challenge for the engineering of osteoinductive materials. It is known that the efficacy of BMP delivery systems depends on the amount of BMP delivered [60] but also on the formulation of the matrix. Commercial collagen matrices are known to poorly retain BMP-2 as 40–60% of the encapsulated protein is immediately released in the first 3 h, leading to low therapeutic effect and cost-effectiveness [61–63]. In order to overcome such drawbacks, several studies have been undertaken with the aim of delivering BMP-2 more efficiently [64–66]. Some of these studies used bulk polymers where considerable amounts of BMP-2 were required (in the order of the milligrams). Recently, hydrogels that present a stronger affinity for BMP-2 have also been developed [67,68].

To our knowledge, very few studies have aimed at delivering BMP-2 from polysaccharide-based membranes. Recently, Chung

S.G. Caridade et al. / Acta Biomaterialia xxx (2015) xxx–xxx
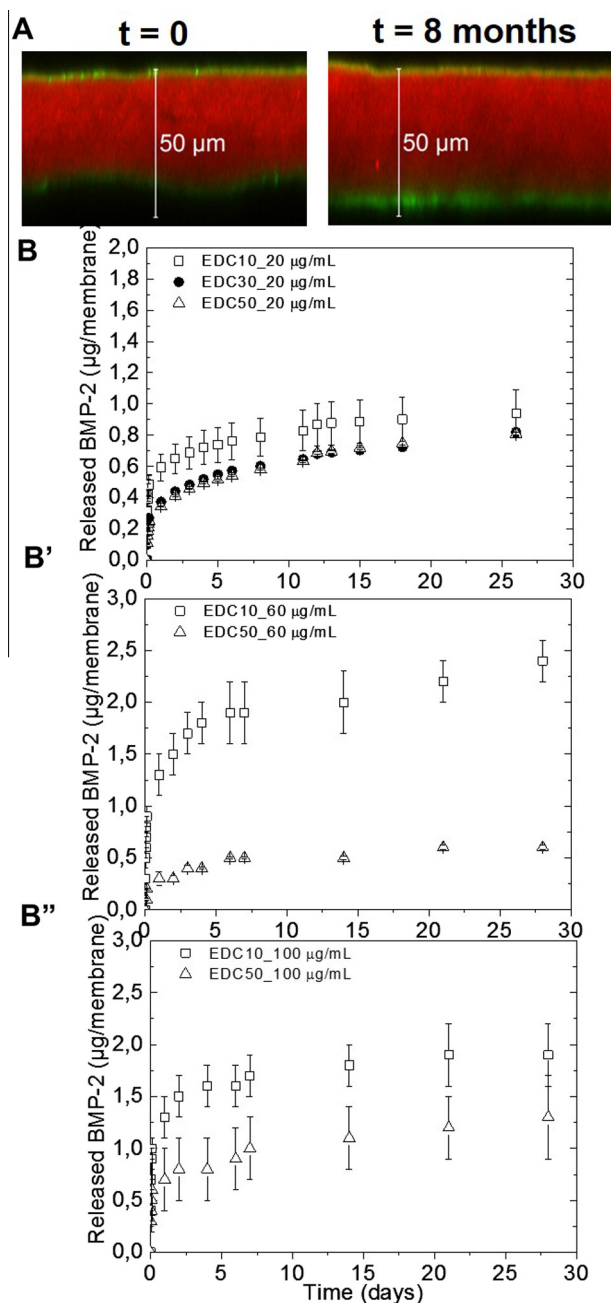
Fig. 4. Quantification of BMP-2 loaded in and released from the (CHI/ALG) FS membranes. (A) CLSM images of the EDC50 FS membrane labeled with Alexa 568 (red) and loaded with BMP-2 ^{CF} (green). Two BMP-2 layers, on the lower and upper side of the membrane, were observed over a period of 8 months. (B) Release profiles of the EDC10, EDC30 and EDC50 FS membranes over a period of 1 month for an initial BMP-2 loading concentration of 20 μg ml^{-1}; (B′, B″) release profiles of the EDC10 and EDC50 FS membranes over a period of 1 month for initial BMP-2 loading concentrations of 60 μg ml^{-1} (B′) and 100 μg ml^{-1} (B″). Values are mean + SEM of three samples.

et al. [69] produced an ~130 μm thick self-assembled membrane made of collagen with HA. The membranes were fabricated in a single step by adding BMP-2 to the collagen solution before overlaying it on top of the HA solution. Chung et al. observed a slow, sustained release of BMP-2 without an initial burst release. Such behavior was attributed to the washing steps necessary to eliminate the excess HA solution immediately upon membrane formation, and to both the physical entrapment of BMP-2 within the collagen–HA membrane and the ionic complexation between the

negatively charged carboxyl groups of HA and the net positively charged BMP-2 protein. Such bonds contributed to enhancing the noncovalent immobilization, prolonged release of the protein and lack of a burst release. The osteogenic potential of collagen–HA membranes at 4 weeks in a subcutaneous mouse model was shown via Von Kossa staining and immunostaining of osteopontin and osteocalcin.

Surface coatings in the form of LbL films can be used to locally deliver BMP-2 from biomaterial surfaces [26,51,70]. The different strategies showed that: (i) the precise film architecture allowed compartmentalization of the protein, leading to sequential release; (ii) the loading of proteins can be done in mild conditions, thus preserving their activity; and (iii) the release can be tuned by the number of layers.

In our previous study [29], we demonstrated that native (CHI/ALG) FS membranes were permeable to FITC–dextran of different molecular weights. Here, we showed that BMP-2 can be loaded in crosslinked FS polysaccharide membranes. The amount loaded can be tuned depending on the initial concentration of BMP-2 in solution and the degree of crosslinking of the FS membrane (Fig. 4 and Table 1). In view of the different parameters used by the different research groups (including the formulation conditions, BMP-2 doses used and loading conditions), it is difficult to correlate our results directly with the other studies. Comparison of the behavior of poly-ʟ-lysine (PLL)/HA films might be more relevant, as we followed the same protocol to load BMP-2 in the EDC-crosslinked FS membranes as was previously used for crosslinked PLL/HA-supported films [26]. In the work of Crouzier et al. [37], the release of BMP-2 loaded at 100 μg ml^{-1} in PLL/HA films deposited on macroporous β-tricalcium phosphate/HA and crosslinked (EDC10 and 50) membranes was followed over 46 days. At the end of the study period, the amounts of BMP-2 retained were 3.2 ± 0.4 and 4.1 ± 0.7 μg per granule for the films crosslinked with EDC10 and EDC50, respectively. Thus, about 75% of the initial amount loaded was released from the crosslinked film with EDC10 and 30% was released from the one with EDC50. In a recent study, a porous titanium implant was coated using the same PLL/HA film [51] crosslinked with EDC (EDC10, EDC30 and EDC70) and loaded with BMP-2 at 20 and 100 μg ml^{-1}. The amount of BMP-2 incorporated could be tuned over a wide range, depending on both the extent of the film crosslinking and the initial BMP-2 concentration. For example, EDC10 incorporated the highest amount of BMP-2 (4.2 and 18.9 μg cm^{-2} when loaded with 20 and 100 μg ml^{-1} of BMP-2, respectively). At the end of 7 days, such EDC10 released 62 and 77% of the initial amount of BMP-2 incorporated for 20 and 100 μg ml^{-1} BMP-2, respectively. The more crosslinked films were found to load more BMP-2 and to release a lower percentage of it. Thus, the incorporation and release profiles we observed here are qualitatively similar, i.e. increased BMP-2 loading with higher initial BMP-2 concentration and increased percentage released with less crosslinked film/membrane (EDC10 compared to EDC50).

Macdonald et al. [71] coated a 3-D scaffold by using LbL films consisting of 100 successively deposited tetralayers. Each tetralayer consisted of a hydrolyzable poly(β-aminoester) as a polycation, chondroitin sulfate as a polyanion and BMP-2 as a polycation at an initial concentration of 50 μg ml^{-1} paired with chondroitin sulfate. A small burst release was observed and 80% of BMP-2 was released over a period of 2 days, with the remaining 20% being released in a sustained way over a period of 2 weeks. Macdonald et al. found that the total amount of BMP-2 could be tuned depending on the number of tetralayers. Other release profiles have also been discussed in the literature [70,72] using the LbL technology.

The loading of BMP-2 in our EDC50 crosslinked FS membranes led to a decrease in cell proliferation after 24 h in culture in GM (Fig. 5A) compared to the case without BMP-2 (Fig. 3). This result

Table 1

Summary table of the initial (Γ_i) and final (Γ_f) adsorbed amount of BMP-2 as well as burst (Γ_{Burst}) and percentage released after 28 days.

[BMP-2]$_{initial}$ (µg ml^{-1})	20				60				100			
Γ (µg)	Γ_i	Γ_f	Γ_{Burst}	% Released	Γ_i	Γ_f	Γ_{Burst}	% Released	Γ_i	Γ_f	Γ_{Burst}	% Released
EDC10	2.7 ± 0.4	1.7 ± 0.3	~0.5	36.9 ± 10.6	7.4 ± 1.8*	5.0 ± 0.2	~0.9	34.3 ± 7.5	10.8 ± 1.2*	8.8 ± 0.3	~1	18.0 ± 3.4
EDC30	3.0 ± 1.0	2.1 ± 0.3	~0.3	29.5 ± 4.8	NA	NA	NA	NA	NA	NA	NA	NA
EDC50	3.9 ± 0.2	3.1 ± 0.3	~0.3	20.8 ± 2.1	4.4 ± 0.6	3.8 ± 0.6	~0.2$	14.4 ± 2.0	8.0 ± 2.6#	7.4 ± 2.3	~0.6	15.0 ± 1.3

The FS membranes crosslinked at EDC10, 30 or 50 were loaded with an initial concentration of BMP-2 of 20, 60 and 100 µg ml^{-1}. $p < 0.05$ (*) when comparing to EDC10 loaded @ 20 µg ml^{-1}; (#) when comparing to EDC50 loaded @ 20 µg ml^{-1}; ($) when comparing to EDC10 loaded @ 60 µg ml^{-1}.
NA: not applicable.
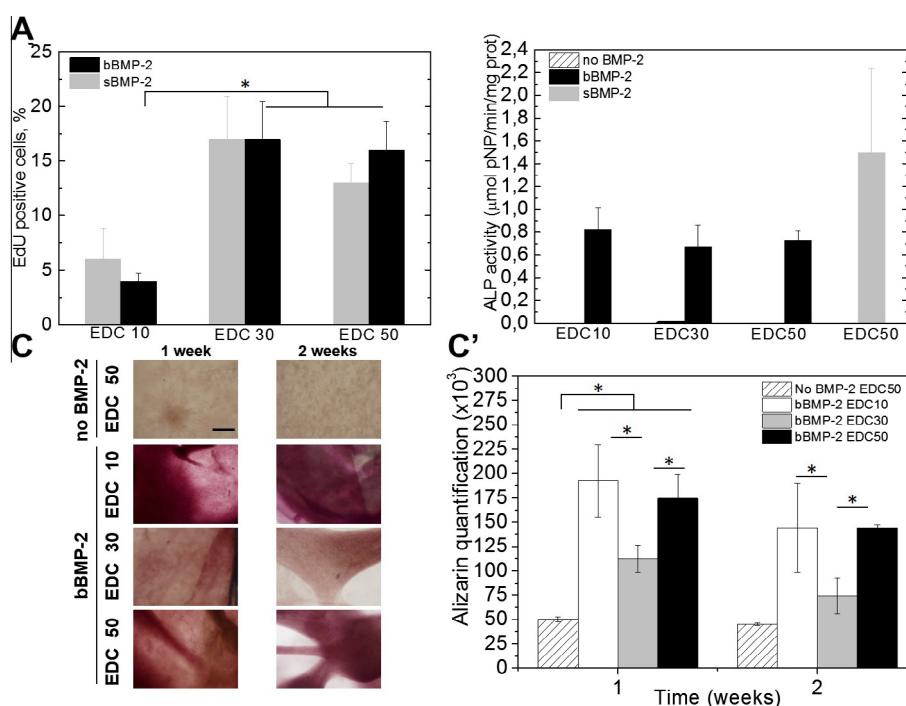
Fig. 5. Proliferation and osteogenic differentiation of C2C12 myoblasts on BMP-2-loaded FS membranes. (A) Quantification of myoblast proliferation after 24 h of culture in GM in the absence or presence of BMP-2 loaded in the FS membranes (triplicate samples, $n = 3$) or added in solution to the cells. (B) ALP activity of C2C12 myoblasts cultured for 3 days on the BMP-2-loaded membranes crosslinked at EDC10, 30 and 50 (BMP-2 was loaded at 20 µg ml^{-1} on the FS membranes) in comparison to an FS membrane in the presence of sBMP-2 (positive control, BMP-2 added at 600 ng ml^{-1}) (triplicate samples, $n = 3$). (C) Microscopic images of Alizarin red staining showing C2C12 cell mineralization in contact with the crosslinked FS membranes after 1 and 2 weeks in culture. Upper panel: myoblasts on FS membranes in the absence of BMP-2, showing no mineralization. Lower panels: cell mineralization on BMP-2-loaded FS membranes, the membranes crosslinked at EDC10, EDC30 or EDC50 ($n = 3$). Scale bar = 200 µm. (C′) Quantification of Alizarin red from groups of pictures shown in (C). *$p < 0.05$.

may be explained by the differentiation commitment of the cells, as they exit the cell cycle to commit to osteogenesis. Indeed, this finding is corroborated with the ALP activity after 3 days in culture. Our results regarding the decrease in proliferation are consistent with the results obtained by Chung et al. [69] for collagen/HA membranes loaded with BMP-2.

The results of the preliminary in vivo study in an ectopic site of nude mice revealed differences between the FS membranes according to their degree of crosslinking and the amount of BMP-2 incorporated. Note that we have already shown that, in the absence of BMP-2, a polysaccharide film cannot itself be osteoinductive [51]. Here, the EDC10 membranes did not lead to a visible bone nodule formation even after 52 days. In contrast, EDC50 membranes led to observable bone formation in the vicinity of the membrane as early as 21 days after implantation (Fig. 6A), but only for the highest BMP-2 loading concentration. In view of the different loading and release profiles of the FS membranes (Table 1 and Fig. 4), several hypotheses may be made: first, these differences in osteoinduction may be due to the different release

kinetics in vivo; second, they may be due to a different bioactivity of the BMP-2 released from the cross-linked membranes; and third, the biodegradability of the FS polysaccharide membranes in vivo may play a role, as in vivo biodegradability of CHI/HA films was previously shown to depend on the degree of crosslinking [25].

Several studies have shown that a carrier incorporating BMP-2 can induce bone formation in an ectopic site by activating a set of cellular events [50,69,71,73,74]. Although all of these studies observed bone formation, the amount of BMP-2 incorporated in the carriers and the time in which osteogenesis occurred were always different. Usually, in vivo experiments using rats (subcutaneous back) and rabbits (intramuscular) as animal models revealed bone formation after 4 weeks. Kisiel et al. [74] using an injectable hyaluronic acid hydrogel as a BMP carrier (20 µg ml^{-1}) in a rat ectopic model, observed bone formation after 7 weeks. Here, we found bone formation at 3 weeks. In all cases, it seems that the induction of bone formation requires a local retention of BMP-2, a release over a prolonged period and exposure to the surrounding cells.

10   *S.G. Caridade et al./Acta Biomaterialia xxx (2015) xxx–xxx*
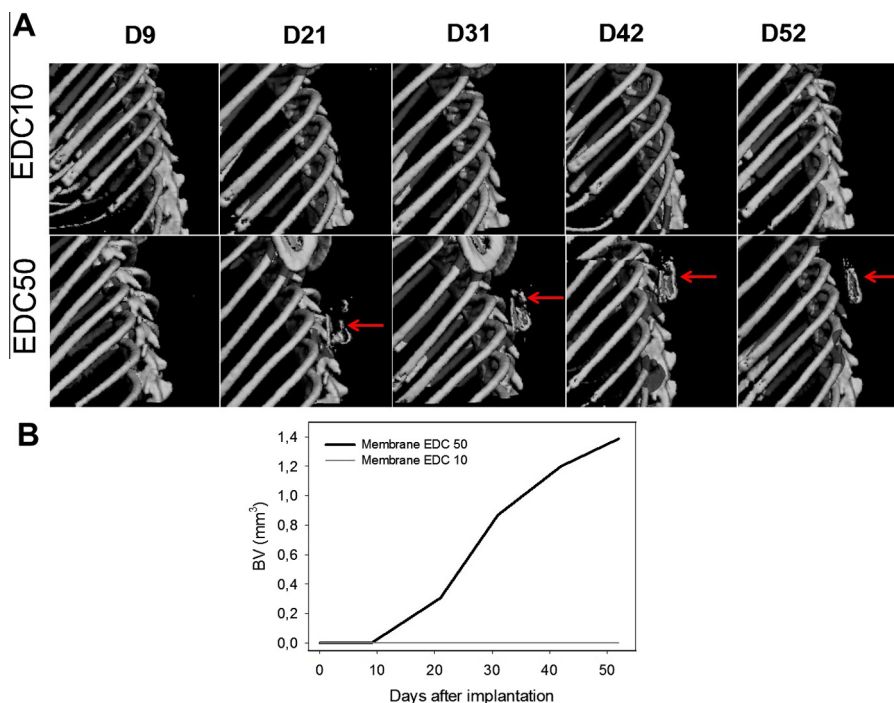
Fig. 6. (A) Time-lapse μCT imaging of bone formation for BMP-2-loaded crosslinked FS membranes implanted under the skin of mice, followed at regular time intervals up to day 52. The bone nodule forming in the case of the EDC50 FS membrane is indicated with a red arrow. (B) Quantification of the bone volume as a function of time for the EDC10 and EDC50 BMP-2-loaded FS membranes. No bone formation was detected for the EDC10 FS membrane.

In future studies, we aim to follow the biodegradability of the FS membrane as well as BMP-2 release in vivo. In addition, the next step will be to study their osteoinductive properties in a bone site.

5. Conclusions

In summary, FS membranes made of the polysaccharides CHI and ALG were crosslinked chemically using EDC, which improved their mechanical properties. The crosslinked membranes enabled the proliferation of skeletal myoblasts and their subsequent differentiation in myotubes, a process that depended on the extent of crosslinking. Furthermore, the crosslinked FS membranes could be loaded with the osteoinductive growth factor BMP-2. The amount of BMP-2 loaded and the release profile were tuned depending on the EDC concentration and the initial concentration of BMP-2 in solution. After an initial burst, the growth factor was released over 1 month by diffusion. The osteoinductive capacity of the FS membranes was proved in vitro by the ALP test and mineralization assays. Preliminary in vivo data suggest that the EDC50 FS membrane was osteoinductive in a mouse ectopic model after 21 days. We believe that these myoconductive and osteoinductive membranes will open new perspectives for future in vivo studies as tissue-engineered constructs for the repair of bone fractures.

Acknowledgements

Appendix A. Figures with essential color discrimination

Certain figures in this article, particularly Figs. 1, 3, 5 and 6 are difficult to interpret in black and white. The full color images can be found in the on-line version, at http://dx.doi.org/10.1016/j.actbio.2014.12.027.

References

[1] Ma PX. Biomimetic materials for tissue engineering. Adv Drug Deliv Rev 2008;60:184–98.

[2] Nikkhah M, Edalat F, Manoucheri S, Khademhosseini A. Engineering microscale topographies to control the cell–substrate interface. Biomaterials 2012;33:5230–46.

[3] Paulsson M. Basement membrane proteins: structure, assembly, and cellular interactions. Crit Rev Biochem Mol 1992;27:93–127.

[4] Sakai D, Kii I, Nakagawa K, Matsumoto HN, Takahashi M, Yoshida S, et al. Remodeling of actin cytoskeleton in mouse periosteal cells under mechanical loading induces periosteal cell proliferation during bone formation. PLoS ONE 2011;6.

[5] Moore SR, Milz S, Tate MLK. Periosteal thickness and cellularity in mid-diaphyseal cross-sections from human femora and tibiae of aged donors. J Anat 2014;224:142–9.

[6] Al-Qtaitat A, Shore RC, Aaron JE. Structural changes in the ageing periosteum using collagen III immuno-staining and chromium labelling as indicators. J Musculoskel Neuron 2010;10:112–23.

[7] Arnsdorf EJ, Jones LM, Carter DR, Jacobs CR. The periosteum as a cellular source for functional tissue engineering. Tissue Eng Part A 2009;15:2637–42.

[8] Chang H, Tate MLK. Concise review: the periosteum: tapping into a reservoir of clinically useful progenitor cells. Stem Cell Transl Med 2012;1:480–91.

[9] Ueno T, Kagawa T, Mizukawa N, Nakamura H, Sugahara T, Yamamoto T. Cellular origin of endochondral ossification from grafted periosteum. Anat Rec 2001;264:348–57.

[10] Cuthbert RJ, Churchman SM, Tan HB, McGonagle D, Jones E, Giannoudis PV. Induced periosteum a complex cellular scaffold for the treatment of large bone defects. Bone 2013;57:484–92.

[11] Shi X, Fujie T, Saito A, Takeoka S, Hou Y, Shu Y, et al. Periosteum-mimetic structures made from freestanding microgrooved nanosheets. Adv Mat 2014;26:3290–6.

[12] Zhao L, Zhao J, Wang S, Xia Y, Liu J, He J, et al. Evaluation of immunocompatibility of tissue-engineered periosteum. Biomed Mater 2011;6.

[13] Rapp SJ, Jones DC, Gerety P, Taylor JA. Repairing critical-sized rat calvarial defects with progenitor cell-seeded acellular periosteum: a novel biomimetic scaffold. Surgery 2012;152:595–605.

[14] Kang Y, Ren L, Yang Y. Engineering vascularized bone grafts by integrating a biomimetic periosteum and β-TCP scaffold. ACS Appl Mater Interfaces 2014;6:9622–33.

[15] Frohberg ME, Katsman A, Botta GR, Lazarovici P, Schauer CL, Wegst UGK, et al. Electrospun hydroxyapatite-containing chitosan nanofibers crosslinked with genipin for bone tissue engineering. Biomaterials 2012;33:9167–78.

[16] Hoffman MD, Benoit DSW. Emerging ideas: engineering the periosteum: revitalizing allografts by mimicking autograft healing. Clin Orthop Relat Res 2013;471:721–6.

[17] Utvag SE, Grundnes O, Reikeras O. Effects of lesion between bone, periosteum and muscle on fracture healing in rats. Acta Orthop 1998;69:177–80.

[18] Decher G, Hong JD, Schmitt J. Buildup of ultrathin multilayer films by a self-assembly process. III. Consecutively alternating adsorption of anionic and cationic polyelectrolytes on charged surfaces. Thin Solid Films 1992;210/211(Part 2):831–5.

[19] Tang ZY, Wang Y, Podsiadlo P, Kotov NA. Biomedical applications of layer-by-layer assembly: from biomimetics to tissue engineering. Adv Mat 2006;18:3203–24.

[20] Boudou T, Crouzier T, Ren K, Blin G, Picart C. Multiple functionalities of polyelectrolyte multilayer films: new biomedical applications. Adv Mat 2010;22:441–67.

[21] Costa RR, Mano JF. Polyelectrolyte multilayered assemblies in biomedical technologies. Chem Soc Rev 2014;43:3453–79.

[22] Crouzier T, Boudou T, Picart C. Polysaccharide-based polyelectrolyte multilayers. Curr Opin Colloid Interface Sci 2010;15:417–26.

[23] Lutkenhaus JL, Hrabak KD, McEnnis K, Hammond PT. Elastomeric flexible free-standing hydrogen-bonded nanoscale assemblies. J Am Chem Soc 2005;127:17228–34.

[24] Schneider A, Francius G, Obeid R, Schwinté P, Hemmerlé J, Frisch B, et al. Polyelectrolyte multilayers with a tunable Young's modulus: influence of film stiffness on cell adhesion. Langmuir 2006;22:1193–200.

[25] Picart C, Schneider A, Etienne O, Mutterer J, Schaaf P, Egles C, et al. Controlled degradability of polysaccharide multilayer films in vitro and in vivo. Adv Funct Mater 2005;15:1771–80.

[26] Crouzier T, Ren K, Nicolas C, Roy C, Picart C. Layer-by-layer films as a biomimetic reservoir for rhBMP-2 delivery: controlled differentiation of myoblasts to osteoblasts. Small 2009;5:598–608.

[27] Lavalle P, Boulmedais F, Ball V, Mutterer J, Schaaf P, Voegel JC. Free standing membranes made of biocompatible polyelectrolytes using the layer by layer method. J Membr Sci 2005;253:49–56.

[28] Larkin AL, Davis RM, Rajagopalan P. Biocompatible, detachable, and free-standing polyelectrolyte multilayer films. Biomacromolecules 2010;11:2788–96.

[29] Caridade SG, Monge C, Gilde F, Boudou T, Mano JF, Picart C. Free-standing polyelectrolyte membranes made of chitosan and alginate. Biomacromolecules 2013;14:1653–60.

[30] Lee K, Silva EA, Mooney DJ. Growth factor delivery-based tissue engineering: general approaches and a review of recent developments. J R Soc Interface 2011;8:153–70.

[31] Hudalla GA, Murphy WL. Biomaterials that regulate growth factor activity via bioinspired interactions. Adv Funct Mater 2011;21:1754–68.

[32] Li RH, Wozney JM. Delivering on the promise of bone morphogenetic proteins. Trends Biotech 2001;19:255–65.

[33] da Silva RMP, Mano JF, Reis RL. Straightforward determination of the degree of N-acetylation of chitosan by means of first-derivative UV spectrophotometry. Macromol Chem Phys 2008;209.

[34] da Silva RMP, Mano JF, Reis RL. Straightforward determination of the degree of N-acetylation of chitosan by means of first-derivative UV spectrophotometry. Macromol Chem Phys 2008;209:1463–72.

[35] Terbojevich M, Cosani A, Muzzarelli RAA. Molecular parameters of chitosans depolymerized with the aid of papain. Carbohydr Polym 1996;29:63–8.

[36] Crouzier T, Picart C. Ion pairing and hydration in polyelectrolyte multilayer films containing polysaccharides. Biomacromolecules 2009;10:433–42.

[37] Crouzier T, Sailhan Fdr, Becquart P, Guillot R, Logeart-Avramoglou D, Picart C. The performance of BMP-2 loaded TCP/HAP porous ceramics with a polyelectrolyte multilayer film coating. Biomaterials 2011;32:7543–54.

[38] Charrasse S, Comunale F, Fortier M, Portales-Casamar E, Debant A, Gauthier-Rouviere C. M-cadherin activates Rac1 GTPase through the Rho-GEF trio during myoblast fusion. Mol Biol Cell 2007;18:1734–43.

[39] Richert L, Boulmedais F, Lavalle P, Mutterer J, Ferreux E, Decher G, et al. Improvement of stability and cell adhesion properties of polyelectrolyte multilayer films by chemical cross-linking. Biomacromolecules 2004;5:284–94.

[40] Picart C, Elkaim R, Richert L, Audoin F, Arntz Y, Da Silva Cardoso M, et al. Primary cell adhesion on RGD-functionalized and covalently crosslinked thin polyelectrolyte multilayer films. Adv Funct Mater 2005;15:83–94.

[41] Tomihata K, Ikada Y. Crosslinking of hyaluronic acid with water-soluble carbodiimide. J Biomed Mater Res 1997;37:243–51.

[42] Taguchi T, Ikoma T, Tanaka J. An improved method to prepare hyaluronic acid and type II collagen composite matrices. J Biomed Mater Res 2002;61:330–6.

[43] Valentin R, Bonelli B, Garrone E, Di Renzo F, Quignard F. Accessibility of the functional groups of chitosan aerogel probed by FT-IR-monitored deuteration. Biomacromolecules 2007;8:3646–50.

[44] Lawrie G, Keen I, Drew B, Chandler-Temple A, Rintoul L, Fredericks P, et al. Interactions between alginate and chitosan biopolymers characterized using FTIR and XPS. Biomacromolecules 2007;8:2533–41.

[45] Mano JF. Viscoelastic properties of chitosan with different hydration degrees as studied by dynamic mechanical analysis. Macromol Biosci 2008;8:69–76.

[46] Alves NM, Ribelles JLG, Tejedor JAG, Mano JF. Viscoelastic behavior of poly(methyl methacrylate) networks with different cross-linking degrees. Macromolecules 2004;37:3735–44.

[47] Urist MR. Bone: Formation by autoinduction. Science 1965;150:893–9.

[48] Wozney JM, Rosen V, Celeste AJ, Mitsock LM, Whitters MJ, Kriz RW, et al. Novel regulators of bone-formation – molecular clones and activities. Science 1988;242:1528–34.

[49] Katagiri T, Yamaguchi A, Komaki M, Abe E, Takahashi N, Ikeda T, et al. Bone morphogenetic protein-2 converts the differentiation pathway of C2C12 myoblasts into the osteoblast lineage. J Cell Biol 1994;127:1755–66.

[50] Hsu HP, Zanella JM, Peckham SM, Spector M. Comparing ectopic bone growth induced by rhBMP-2 on an absorbable collagen sponge in rat and rabbit models. J Orthop Res 2006;24:1660–9.

[51] Guillot R, Gilde F, Becquart P, Sailhan F, Lapeyrere A, Logeart-Avramoglou D, et al. The stability of BMP loaded polyelectrolyte multilayer coatings on titanium. Biomaterials 2013;34:5737–46.

[52] Augustin G, Antabak A, Davila S. The periosteum. Part 1. Anatomy, histology and molecular biology (Retracted Article. See vol. 39, p. 824, 2008). Injury-Int J Care Injured 2007;38:1115–30. Q11

[53] Andrés V, Walsh K. Myogenin expression, cell cycle withdrawal, and phenotypic differentiation are temporally separable events that precede cell fusion upon myogenesis. J Cell Biol 1996;132:657–66.

[54] Rowley JA, Mooney DJ. Alginate type and RGD density control myoblast phenotype. J Biomed Mater Res 2002;60:217–23.

[55] Boontheekul T, Hill EE, Kong HJ, Mooney DJ. Regulating myoblast phenotype through controlled gel stiffness and degradation. Tissue Eng 2007;13:1431–42.

[56] Rossi CA, Pozzobon M, De Coppi P. Advances in musculoskeletal tissue engineering moving towards therapy. Organogenesis 2010;6:167–72.

[57] Engler AJ, Griffin MA, Sen S, Bönnemann CG, Sweeney HL, Discher DE. Myotubes differentiate optimally on substrates with tissue-like stiffness: pathological implications for soft or stiff microenvironments. J Cell Biol 2004;166:877–87.

[58] Gilbert PM, Havenstrite KL, Magnusson KEG, Sacco A, Leonardi NA, Kraft P, et al. Substrate elasticity regulates skeletal muscle stem cell self-renewal in culture. Science 2010;329:1078–81.

[59] Ren K, Crouzier T, Roy C, Picart C. Polyelectrolyte multilayer films of controlled stiffness modulate myoblast cell differentiation. Adv Funct Mater 2008;18:1378–89.

[60] Wozney JM, Rosen V, Byrne M, Celeste AJ, Moutsatsos I, Wang EA. Growth factors influencing bone development. J Cell Sci 1990;1990:149–56.

[61] Uludag H, Gao T, Porter TJ, Friess W, Wozney JM. Delivery systems for BMPs: factors contributing to protein retention at an application site. J Bone Joint Surg 2001;83:S128–35.

[62] Zara JN, Siu RK, Zhang XL, Shen J, Ngo R, Lee M, et al. High doses of bone morphogenetic protein 2 induce structurally abnormal bone and inflammation in vivo. Tissue Eng Part A 2011;17:1389–99.

[63] Carragee EJ, Hurwitz EL, Weiner BK. A critical review of recombinant human bone morphogenetic protein-2 trials in spinal surgery: emerging safety concerns and lessons learned. Spine J 2011;11:471–91.

[64] Geiger M, Li RH, Friess W. Collagen sponges for bone regeneration with rhBMP-2. Adv Drug Deliv Rev 2003;55:1613–29.

[65] Li C, Vepari C, Jin H-J, Kim HJ, Kaplan DL. Electrospun silk-BMP-2 scaffolds for bone tissue engineering. Biomaterials 2006;27:3115–24.

[66] Kempen DHR, Lu L, Hefferan TE, Creemers LB, Maran A, Classic KL, et al. Retention of in vitro and in vivo BMP-2 bioactivities in sustained delivery vehicles for bone tissue engineering. Biomaterials 2008;29:3245–52.

[67] Kisiel M, Martino MM, Ventura M, Hubbell JA, Hilborn J, Ossipov DA. Improving the osteogenic potential of BMP-2 with hyaluronic acid hydrogel modified with integrin-specific fibronectin fragment. Biomaterials 2013;34:704–12.

[68] Martinez-Sanz E, Ossipov DA, Hilborn J, Larsson S, Jonsson KB, Varghese OP. Bone reservoir: injectable hyaluronic acid hydrogel for minimal invasive bone augmentation. J Control Release 2011;152:232–40.

[69] Chung EJ, Chien KB, Aguado BA, Shah RN. Osteogenic potential of BMP-2-releasing self-assembled membranes. Tissue Eng Part A 2013;19:2664–73.

[70] Shah NJ, Macdonald ML, Beben YM, Padera RF, Samuel RE, Hammond PT. Tunable dual growth factor delivery from polyelectrolyte multilayer films. Biomaterials 2011;32:6183–93.

[71] Macdonald ML, Samuel RE, Shah NJ, Padera RF, Beben YM, Hammond PT. Tissue integration of growth factor-eluting layer-by-layer polyelectrolyte multilayer coated implants. Biomaterials 2011;32:1446–53.

[72] Shah NJ, Hong J, Hyder MN, Hammond PT. Osteophilic multilayer coatings for accelerated bone tissue growth. Adv Mat 2012;24:1445–50.

[73] Yamamoto M, Takahashi Y, Tabata Y. Controlled release by biodegradable hydrogels enhances the ectopic bone formation of bone morphogenetic protein. Biomaterials 2003;24:4375–83.

[74] Kisiel M, Ventura M, Oommen OP, George A, Walboomers XF, Hilborn JN, et al. Critical assessment of rhBMP-2 mediated bone induction: an in vitro and in vivo evaluation. J Control Release 2012;162:646–53.